Results in Engineering 24 (2024) 102922

Contents lists available at ScienceDirect

Results in Engineering

journal homepage: www.sciencedirect.com/journal/results-in-engineering

Co_3O_4 nanoparticles synthesized with rotten-grape extract for use in supercapacitors and oxygen evolution devices

Asma Hayat [a], Aneela Tahira [b], Muhammad Ali Bhatti [c], Irum Naz [a], Aqeel Ahmed Shah [f], Elmuez Dawi [d,*], Matteo Tonezzer [g], Ayman Nafady [e], Riyadh H. Alshammari [e], Zafar Hussain Ibupoto [a,**]

[a] Institute of Chemistry, University of Sindh, Jamshoro, 76080, Pakistan
[b] Institute of Chemistry, Shah Abdul Latif University Khairpur Mirs, Sindh, Pakistan
[c] Centre for Environmental Sciences, University of Sindh, Jamshoro, 76080, Sindh, Pakistan
[d] College of Humanities and Sciences, Department of Mathematics and Sciences, Ajman University, P.O.Box 346, Ajman, United Arab Emirates
[e] Chemistry Department, College of Science, King Saud University, Riyadh, 11451, Saudi Arabia
[f] Wet Chemistry Laboratory, Department of Metallurgical Engineering, NED University of Engineering and Technology, University Road, Karachi, 75270, Pakistan
[g] Department of Chemical and Geological Sciences, University of Cagliari, Monserrato, Italy

ARTICLE INFO

Keywords:
Rotten grape fruit juice
Co_3O_4 nanostructures
Supercapacitor
Oxygen evolution reaction
Alkaline electrolyte

ABSTRACT

Phytochemicals in grape fruit juice have never been considered as potential sources of surface modification, shape modification, and energy storage. In our study, we demonstrate the hydrothermal synthesis of Co_3O_4 nanostructures from grape fruit extracts. X-ray diffraction analysis revealed that Co_3O_4 nanostructures exhibit a cubic phase, while Fourier transform infrared spectroscopy identified several functional groups. An analysis of Co_3O_4 nanostructures using a scanning electron microscope revealed that uniformly distributed nanoparticles of Co_3O_4 were trapped in the carbon content of the spices during calcination. UV–visible spectrometer analysis of Co_3O_4 nanostructures reveals a wide range of optical bands. It was found that one mL of grape fruit juice provided the lowest optical band gap of 2.51 eV for Co_3O_4 nanostructures. Nanostructures of Co_3O_4 were studied under alkaline conditions for use in supercapacitors and oxygen evolution reactions. An aqueous solution containing 1 mL of assisted Co_3O_4 nanostructures exhibited an overpotential of 290 mV at a current density of 10 mA cm^{-2} in 1 M KOH. In addition, they showed a Tafel slope of 80 mV dec^{-1}. When dissolved in 3 M KOH electrolyte, grape fruit juice assisted Co_3O_4 nanostructures showed a specific capacitance of 867 F/g at 1.5 A/g in 3 M KOH aqueous solution. A specific capacitance retention percentage of about 101.1 % was achieved after 40000 galvanic charge-discharge cycles. It has been shown that the total photochemistry of biomass waste can be tuned and enhanced to enhance the functional properties of nanostructures derived from rotten grape fruit extract in order to develop functional materials with high performance for a wide range of applications.

1. Introduction

Throughout the modern industrial sector, the intensive revolution has resulted in an increased demand for a wide variety of energy sources. This gesture has not only resulted in a rapid decline in energy reserves, but has also caused significant environmental damage, both intentionally and unintentionally [1–4]. There is growing interest in electrochemical water splitting as a potential technology for producing high density green hydrogen fuels [5]. Contrary to this, the water splitting process makes use of two different types of half-cell reactions, namely oxygen evolution reactions (OERs) at the cathode and hydrogen evolution reactions (HERs) at the anode [6]. Due to the four-electron transfer process, the OER process is associated with slow kinetics and has therefore prevented the full utilization of water splitting for efficient hydrogen production [6,7]. The current state-of-the-art electrocatalysts for the OER process have been noble metal catalysts, particularly RuO_2 and IrO_2, although their large-scale utilization has been prohibited because of their feared nature, high costs, and certain stability issues

* Corresponding author.
** Corresponding author.
E-mail addresses: e.dawi@ajman.ac.ae (E. Dawi), zaffar.ibhupoto@usindh.edu.pk (Z.H. Ibupoto).

https://doi.org/10.1016/j.rineng.2024.102922
Received 20 June 2024; Received in revised form 31 August 2024; Accepted 16 September 2024
Available online 17 September 2024
2590-1230/© 2024 The Authors. Published by Elsevier B.V. This is an open access article under the CC BY-NC-ND license (http://creativecommons.org/licenses/by-nc-nd/4.0/).

under harsh electrolytic conditions [8]. Thus, there is a substantial amount of literature on the design and manufacture of electrocatalysts that are cost-effective, earth-abundant, stable, scalable, and efficient. In light of the heterogeneous distribution of renewable energy resources, effective and efficient energy storage systems are urgently needed [9,10]. The development of supercapacitors (SCs) has recently emerged as one of the most innovative energy storage devices and has been receiving considerable attention around the world. It is argued that the main characteristics of SCs are their high specific power density of approximately 10 kW/kg, their fast charging and discharging abilities within a few seconds, and their high cycling stability of approximately 105 times that of lithium ion batteries [11]. These attractive and unique characteristics of SCs make them a very important source of energy in a variety of fields, including mobile electric systems, backup power, power plants, military equipment, and hybrid electric cars [12]. The only disadvantage of SCs is their low energy density, which is approximately 3–6 Wh/Kg, compared to lithium ion batteries that are approximately 150–200 Wh/Kg. Therefore, researchers have conducted studies around the world in order to construct SCs with high energy density [13]. In order to achieve high performance SCs, efficient electrode materials have been required, and materials selection has been based on three main categories, the first being carbonaceous materials [14,15], the second being conducting polymeric compounds [16,17], and the third being transition metal oxides [18]. The carbonaceous materials have been tested as electrode materials for SCs, but their specific capacitance values are less than 400 F/g [19,20]. As alternative and promising electrode materials for pseudo capacitance applications, transition metal oxides and conducting polymeric compounds have been investigated [21]. As a result of contraction and expansion during charging and discharging, conducting polymers do not possess an extremely stable specific capacitance of less than 530 F/g on average [22]. It has been demonstrated that transition metal oxides exhibit fast Faradaic reactions as well as high specific capacitances when they are intrinsically enhanced with variable oxidation states [23]. In contrast, transition metal oxides have been used to split water in OER half-cells to a greater extent, but their performance has been limited so far [24]. Transition metal oxides, despite their outstanding electrochemical properties, have a poor electrical conductivity due to their wide band gaps, which range between 3 and 4 eV [25]. Due to the tunable engineering of d-orbital electrons in spinel Co3O4, this material provides numerous catalytic sites for a wide range of electrochemical reactions [26–29]. The performance of Co_3O_4 is limited by its low surface area, poor electrical conductivity, and particle aggregation. Co_3O_4 has therefore been prepared by a variety of methods, including co-precipitation, sol-gel, wet chemistry, microwave, electrochemical, hydrothermal, reverse micelles, and green approaches [30–36]. It has been found that physical and chemical methods for synthesis of nanostructures are relatively costly and environmentally harmful [37–40]. Recent studies have focused on the green synthesis of Co_3O_4 using different plant extracts. Plant extracts contain flavonoids, glycosides, and polyphenols that reduce and stabilize nanostructures in a dynamic manner, controlling their size, surface area, and shape. The preparation of Co_3O_4 can be accomplished by utilizing a variety of plant extracts [41–43]. Catechins, flavonoids, and polyphenols are found in high concentrations in grape extract [44]. The grape fruit is composed of three parts: pulp, skin, and seeds. The presence of polyphenols in grape fruit has made it useful in reducing noble metal ions, ketones, and nitrogen compounds. Nanoparticles of gold and silver have been prepared using grape fruit extract [45]. Researchers have synthesized graphene oxide nanocomposites using grape fruit extract [46]. There are no reports that have involved the direct use of rotten grape fruit juice extract to enhance the surface and shape properties of metal oxides. Rotten grape juice has an attractive phytochemistry, including pulp, skin, and seeds. As these phytochemicals with a tendency of reducing, stabilizing, and capping agents are extracted from rotten grape fruit juice, they can potentially change the surface properties with enriched active sites, shape orientation, and particle size in order to enhance electrochemical activity.

Therefore, this study used the rotten grape fruit juice extract is used to prepare surface modified and controlled Co_3O_4 nanostructures that possess improved electrical conductivity, surface area, and catalytic sites for the efficient use of pseudo capacitance and half-cell water splitting with OER. Using rotten gape fruit juice extract, this study investigated how rotten gape fruit extract interacts with Co_3O_4 nanostructures to modify their surface properties. The shape, crystal structure, chemical composition, optical properties, and chemical vibrations of Co_3O_4 nanostructures have been studied using a variety of analytical techniques. It was proposed that modified Co_3O_4 nanostructures could be useful for electrochemical water splitting in alkaline conditions, particularly in asymmetric devices and for OER applications.

2. Materials and method

2.1. Chemical reagents

All the chemical such as cobalt chloride hexahydrate (98 %), urea (99 %), potassium hydroxide (85 %) and Nafion (5 %) were purchased from sigma Aldrich, Karachi Sindh Pakistan.

2.2. Synthesis of Co_3O_4 using rotten grape juice by hydrothermal method

A hydrothermal method was used to prepare nanostructures of cobalt oxide. To grow pristine Co_3O_4, cobalt chloride and urea at a concentration of 0.1M were added to 200 mL deionized water, while growth solutions containing 1 mL and 2 mL of rotten grape fruit juice were also added separately to two beakers labeled sample 1 and sample 2. A pristine sample of Co_3O_4 nanostructures was prepared without adding rotten grape fruit juice. We obtained the rotten grape fruit juice extract by heating 250 g of grapes in 300 mL of deionized water for 3 h at 70 °C. All samples of growth solutions were tightly wrapped in aluminum foil and kept at 95 °C for 5 h. Following filtration, the products were dried at room temperature before being collected. As part of the annealing process, the samples were placed in a furnace at 500 °C for 5 h. A scanning electron microscope (SEM) was used to study the morphology of samples in addition to X-ray diffraction to determine the crystal structure. A UV–visible spectrophotometer was used to measure the band gap energy. Fourier transform infrared (FTIR) spectroscopy was used to elucidate the nature of functional groups on the surface of as synthesized Co_3O_4 nanostructures. Scheme 1 shows the stepwise synthesis of Co_3O_4 nanostructures using rotten grape fruit extract.

2.3. Electrochemical measurement

Electrochemical measurements were conducted using a Versa Potentiostat, including cyclic voltammetry (CV), linear sweep voltammetry (LSV), electrochemical impedance spectroscopy (EIS), chronoamperometry, and chronopotentiometry. We used a three-electrode setup consisting of calomel Hg/HgO as a reference electrode, glassy carbon as a working electrode, and platinum wire as a counter electrode. A mixture of 10 mg of catalyst in 2 mL of deionized water and 50 μL of Nafion solution was prepared by mixing and stirring for 15–20 min, then homogenous catalyst was obtained which was deposited on a working electrode and 1 M KOH was used as an electrolyte. Cyclic voltammetry was used to confirm the stability of the material. A linear sweep voltammetry was performed at 5 mV/s in order to confirm the activity of the OER. To measure the electrochemical surface area, cyclic voltammetry was performed at different scan rates. For the deposition of Co_3O_4 nanostructures onto the nickel foam as an electrode material using same catalyst solution via dip coat method followed by the low temperature sintering method at 80°C for 30 min. Below Scheme 2 is showing the electrochemical measurement used methodology started making catalyst slurry to depositing to the Co_3O_4 nanostructures onto glassy carbon

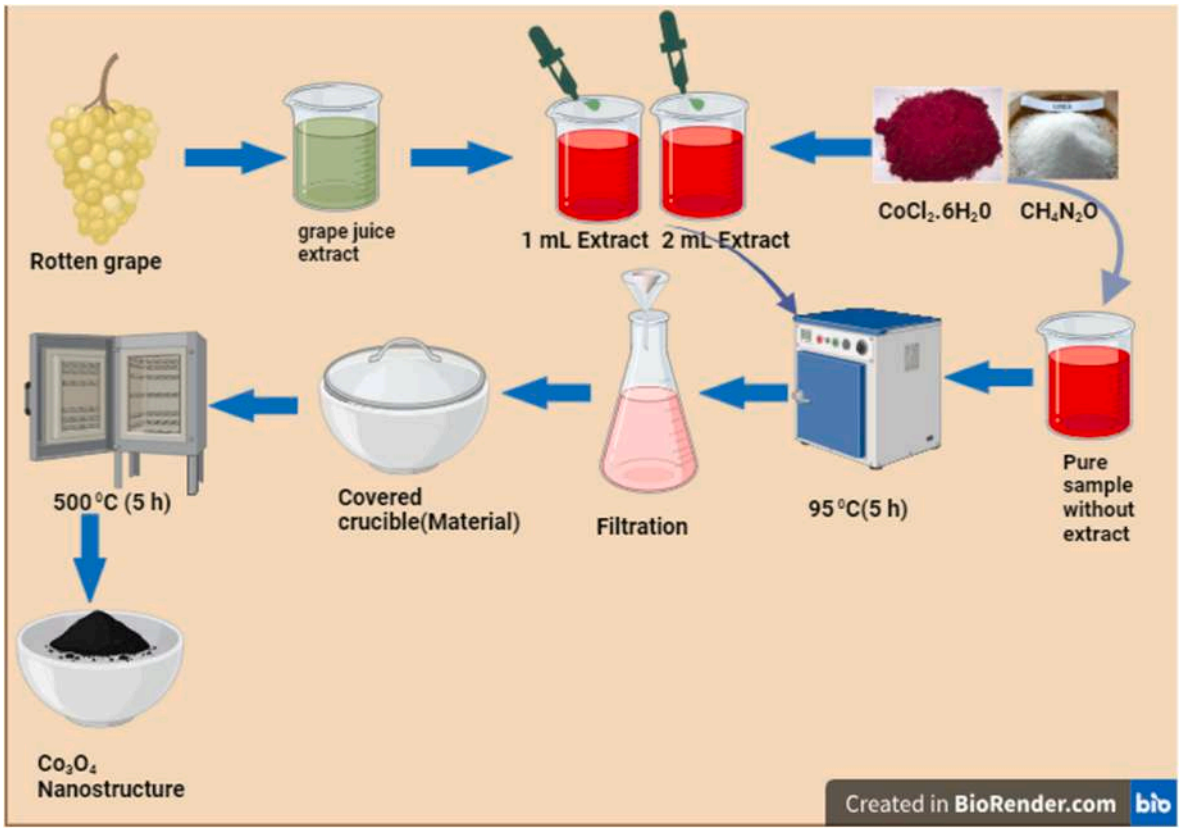

Scheme 1. Schematic Illustration of Hydrothermal process and each step involved in the synthesis of Co3O4 nanostructures using Rotten Grape.

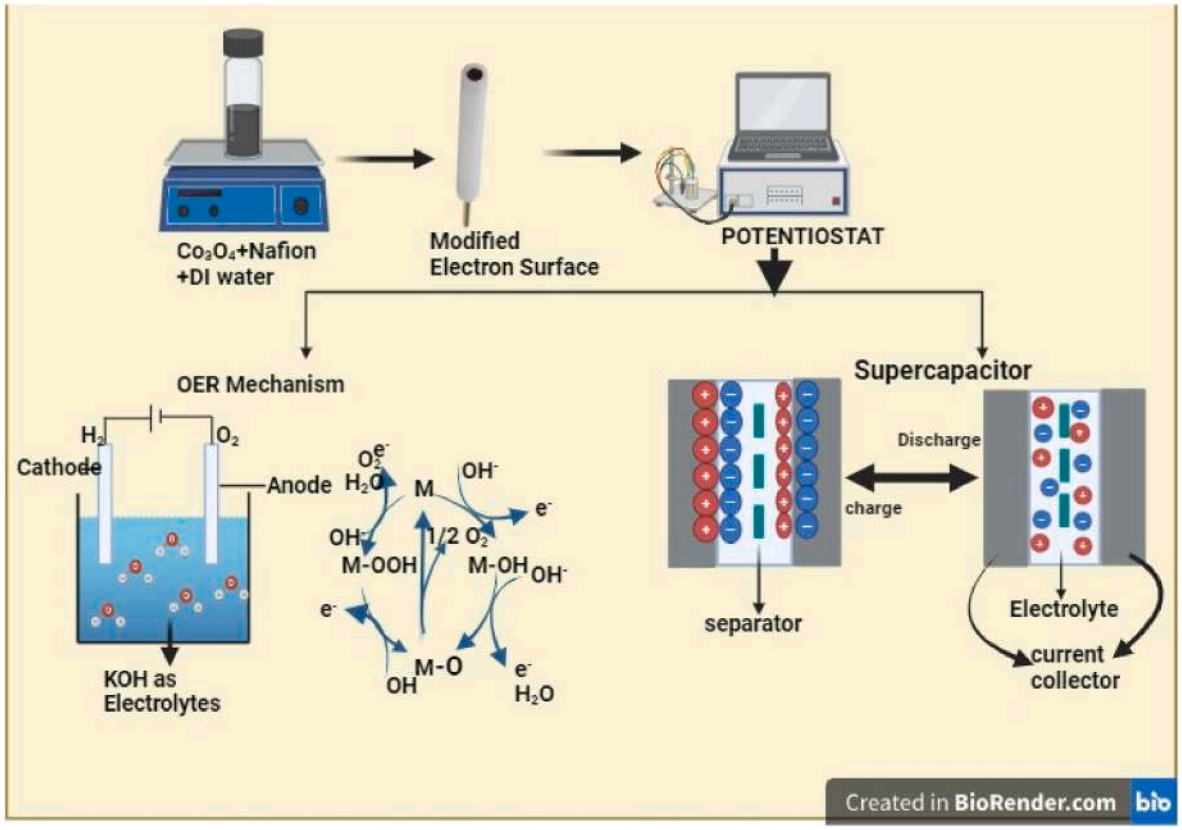

Scheme 2. Schematic Illustration for modification of electrode, the capacitance behavior of Co_3O_4 nanostructures and OER mechanism in alkaline conditions.

electrode and energy conversion and storage uses.

3. Results and discussion

3.1. Structure, shape and optical studies of rotten grape fruit extract derived Co_3O_4 nanostructures

According to Fig. 1, powder X-ray diffraction (XRD) was utilized to identify the reflections of Co_3O_4 nanostructures formed by grape fruit juice phytochemicals. We have found that the diffraction patterns of gape fruit-mediated Co_3O_4 nanostructures, particularly sample 1, are identical to those reported in standard JCPDS card no: 01-074-1656. However, the use of 2 mL of grape juice resulted in the poor crystallization properties of Co_3O_4 nanostructures and the presence of impurities in sample 2. At two-theta indices, it was observed that reflections corresponding to 111, 220, 311, 222, 400, 511, 440, 531, and 442 were located at 18.90, 31.29, 36.81, 38.54, 44.80, 59.37, 65.27, 68.44, and 71.51° for both the pure Co_3O_4 nanostructures and sample 1. The XRD analysis of the presented Co_3O_4 nanostructures, including pure Co_3O_4 nanostructures and sample 1, indicated that all reflection peaks were associated with the cubic phase. Despite this, sample 2 of Co_3O_4 nanostructures exhibits a few patterns that are similar to those of pure Co_3O_4 nanostructures and sample 1. Based on the published results [47–49], the XRD results of pure Co_3O_4 nanostructures and sample 1 were fully consistent. In sample 2, grape fruit extract has caused a significant amount of phytochemicals to be produced during the synthesis of Co_3O_4, leading to changes in crystal nucleation. Phytochemicals in grape fruit juice have strong reducing agents, as a result of which a large alteration in two-theta has been observed. It was observed that sample 2 has a relatively low contribution of Co_3O_4. It may be that the peak at 42.22° is due to the large amount of phytochemicals supplied by the 2 mL of rotten fruit extract in sample 2. Therefore, because of this impurity, sample 2 could not be used to enhance electrochemical activity. Due to their stress, the two-theta shift in the XRD patterns may be caused by the phytochemical compounds such as sugar, invert sugar, dextrose, and glucose solids in grapefruit juice.

Nanostructured materials perform electrochemically differently depending on their size and morphology. Fig. 2 shows the measured SEM images of the synthesized Co_3O_4 nanostructures. In Fig. 2a, it can be seen that the pristine Co_3O_4 nanostructures were oriented into nanowires consisting nanoparticle shapes with heterogeneous size distributions. According to Fig. 2b–c, the grape fruit assisted Co_3O_4 nanostructures (sample 1) were uniform in size. Co_3O_4 nanostructures containing nanoparticles typically have a size between 100 and 200 nm. A cluster of Co_3O_4 nanostructures with a non-homogeneous size distribution is shown in Fig. 2d–e in a 2 mL grape fruit extract. Sample 2 particles were relatively large in size compared to sample 1 due to possible large amounts of phytochemicals in the grape fruit juice, which increased the nucleation rate, resulting in clustered particles with a non-homogeneous distribution of size, as can be seen in Fig. 2d–e. Phytochemical compounds in grape fruit extract vary in amounts, resulting in significant differences in size and shape orientation of Co_3O_4 nanostructures. When the plant or fruit extract is used, a certain amount of carbon can be produced in the metal oxides, thereby eliminating particle agglomeration and aggregation during the process of making catalyst ink for electrode modification, and thus result in a higher level of electrochemical activity. As another point, the grape fruit extract has shown a uniform surface and modified catalytic sites which together can play a dynamic role in facilitating rapid electrochemical reactions. A typical synthesis mechanism can be proposed based on the role of cobalt and hydroxide ions furnished by the cobalt chloride hexahydrate and urea in aqueous solution respectively. The urea hydrolyzed during growth process into ammonia and carbon dioxide, then ammonia reacts with water and produced the ammonium and hydroxide ions as shown in equations 1 and 2. Afterwards, the cobalt ions from aqueous solution reacted with hydroxide ions and produce cobalt hydroxide phase as shown in equation 3. The capped and stabilized Co_3O_4 nanostructures were obtained by thermal annealing of cobalt hydroxide phase at 500°C for 5 h in air as shown in equation 4. The possible role of biomolecules from the rotten grape fruit extract during the synthesis of Co_3O_4 nanostructures was assigned to their behavior as capping, reducing and stabilizing agents. These biomolecules played a vital role in changing the nucleation rate and offering the different binding groups to cobalt ions in addition of hydroxide ions, thus the shape orientation of Co_3O_4 nanostructures was strongly altered.

$$NH_2CONH_2 + H_2O \longrightarrow 2NH_3 + CO_2 \quad (1)$$

$$NH_3 + H_2O \longrightarrow NH_4^+ + OH^- \quad (2)$$

$$Co^{+2} + OH^- + (\text{Biomolecules}) \longrightarrow Co(OH)_2 \quad (3)$$

$$3Co(OH)_2 \xrightarrow[5hr\ in\ air]{500\ ^oC} Co_3O_4\ NP\ (\text{Capped and stabilized}) + 2H_2O + 2O_2 \quad (4)$$

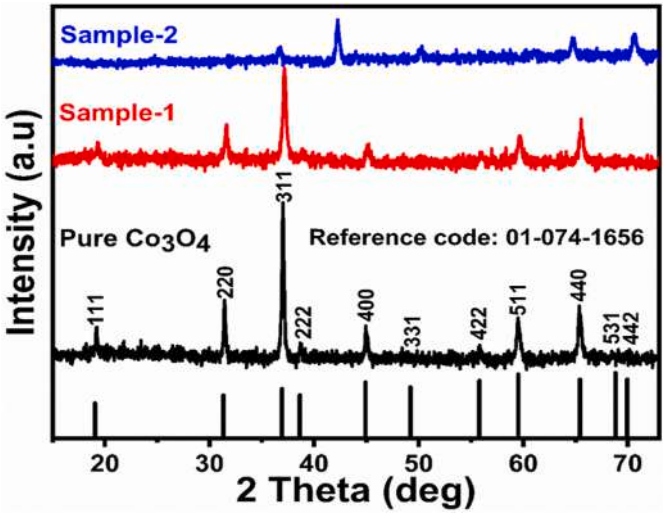

Fig. 1. Powder XRD reflections of Co_3O_4 synthesized with 1 mL and 2 mL of rotten grape (sample 1 and sample 2) and without rotten grape (pureCo_3O_4).

Using energy dispersive spectroscopy (EDS), the elements of pure Co_3O_4 nanostructures, sample 1 and sample 2 were analyzed. As can be seen in Fig. 3a-c, all the samples were characterized with the three major elements Co, O and C. Nevertheless, the relative atomic weight % indicated that sample 1 is associated with more oxygen vacancies, hence possibly playing a vital role in improving the electrochemical performance of the material. Fig. 4a–f shows the EDS mapping of pure Co_3O_4 nanostructures, sample 1 and sample 2 and uniform distribution of Co, O and C could be seen. To determine which functional groups the prepared materials carried, Fourier transform infrared spectroscopy (FTIR) was employed. Thus, FTIR spectra were recorded for pristine Co_3O_4 nanostructures, 1 mL, and 2 mL grape fruit extract-assisted Co_3O_4 nanostructures (Fig. 5). FTIR studies have clearly defined the different types of IR bands visible, particularly those associated with hydroxyl and M − O stretching vibrations. Co-O chemical bonds typically exhibit a strong stretching vibration between 570 and 590 cm^{-1} [50,51]. A major band for the pure Co_3O_4 nanostructures, sample 1 and sample 2 was noticed at 587, 581, and 583 cm^{-1} respectively. Accordingly, the FTIR spectrum of Co_3O_4 nanostructures shows the bending and stretching vibrations for the adsorbed OH hydroxyl group are indexed at 1745 cm^{-1}, as shown in Fig. 5. Phytochemical surface modification of Co_3O_4 nanostructures reduces the relative vibration bands intensity for the OH group. Furthermore, the bands between 904 cm^{-1} were related to O-H-Co stretching vibrations. Few bands between 904 and 751 cm^{-1} possibly could be labeled to different carbon based vibrations emerged from the phytochemicals of rotten grape fruit extract. The stretching band for

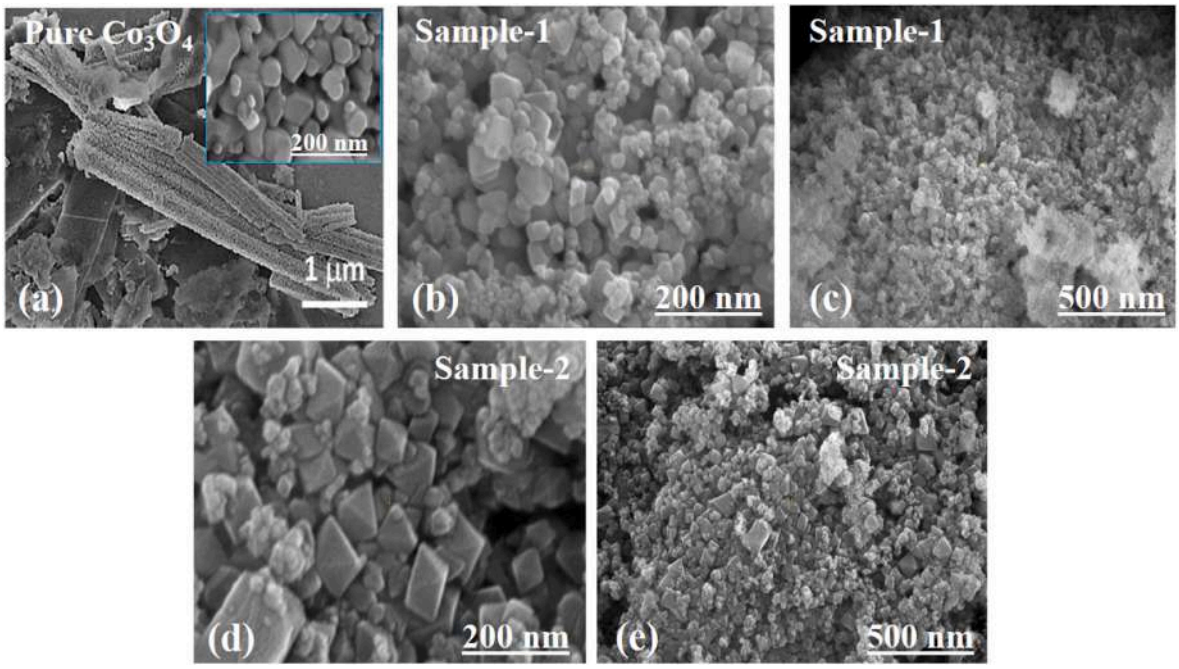

Fig. 2. SEM images (a) pure Co_3O_4, (b.c) 1 mL and 2 mL of rotten grape (sample 1 and sample 2) assisted Co_3O_4.

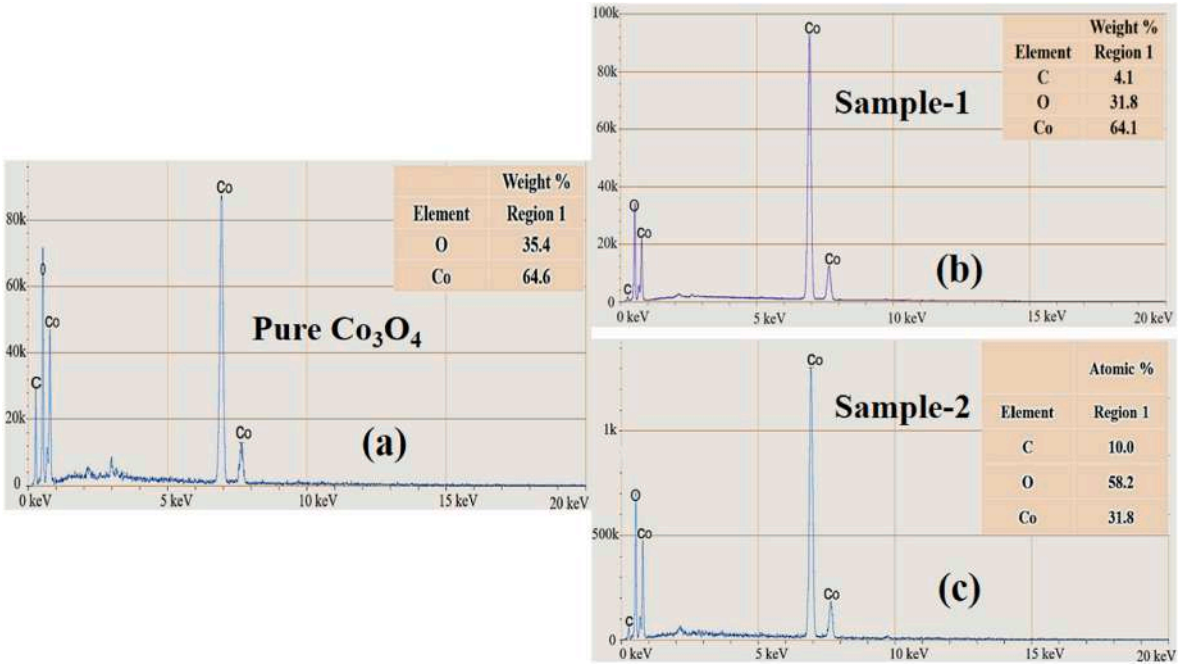

Fig. 3. EDS images (a) pure Co_3O_4, (b.c) 1 mL and 2 mL of rotten grape (sample 1 and sample 2) assisted Co_3O_4.

–OH and $–NH_2$ was noticed at 3106 cm^{-1} due to phytochemicals and surface adsorbed water molecules. Two unidentified bands were noticed at 2671 cm^{-1} and 1904 cm^{-1}. The Co_3O_4 nanostructures based on sample 1 and sample 2 were exhibiting the most of the IR bands with slight variation. As a result of grape fruit juice extract, the frequency positions for functional groups have been slightly altered. UV–visible spectrophotometers have been used to investigate the fundamental optical properties of semiconducting materials. The UV–visible spectra of pure and grape fruit extract supported Co_3O_4 nanostructures were measured, as shown in Fig. 6a. The results confirmed that grape fruit extract significantly affects absorbance values. An intriguing feature of the absorption spectra is the presence of two distinct absorption edges located in the visible region as a result of two oxidation valences of cobalt in Co_3O_4 nanostructures that cause transmission from ($O_2^- \rightarrow Co_2^+$) and ($O_2^- \rightarrow Co_3^+$) [52]. We calculated the optical band gap values using Tauc Equation (1) [53,54].

$$(\alpha h\nu)n = A\ A(h\nu - Eg) \quad (5)$$

Here, $h\nu$ is energy of photons, n and A are constants, and E_g associated to band gap energy and α absorption coefficient. Tauc plots of pure and grape fruit derived Co_3O_4 nanostructures were used to extract the optical band gap value using extrapolated linear plots. Several factors

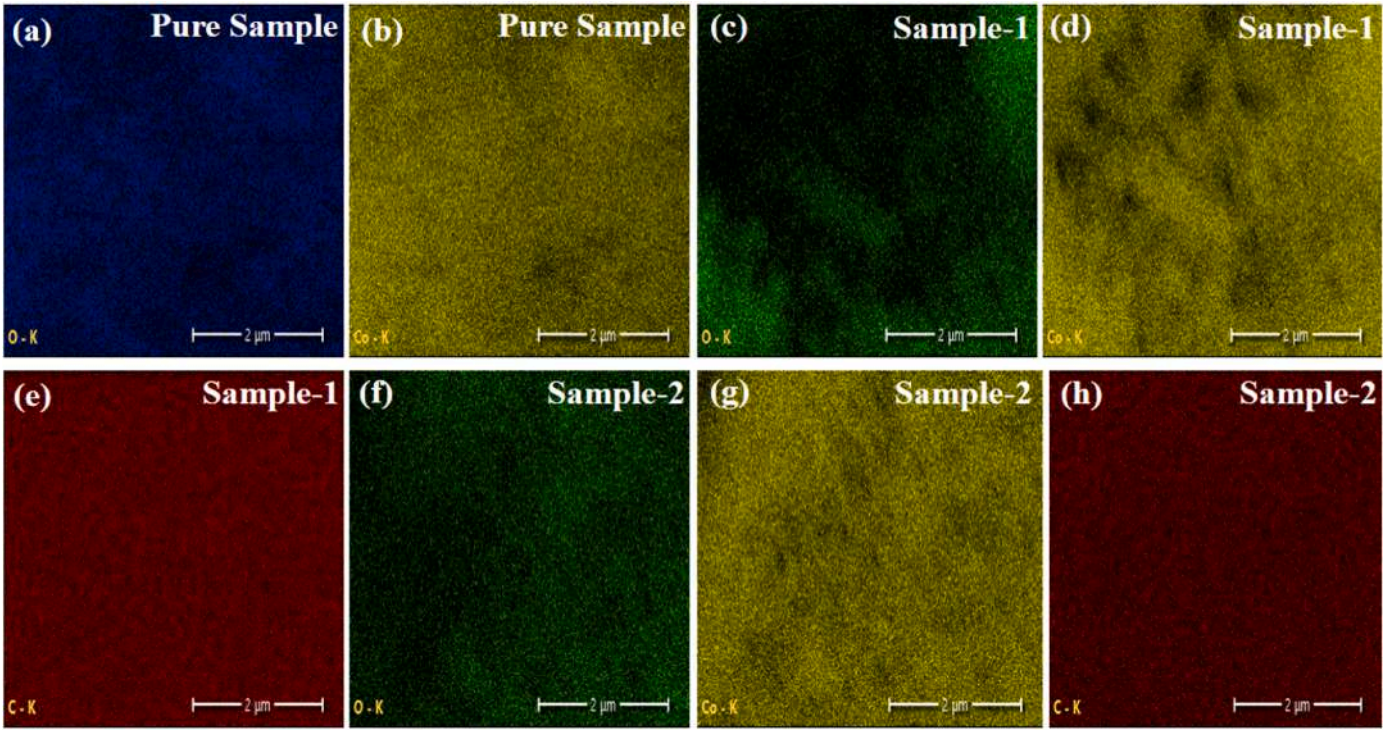

Fig. 4. EDS mapping of (a,b) pure Co_3O_4 nanostructures, (c–e) Co_3O_4 nanostructures prepared with 1 mL and (f–h) 2 mL of sugarcane molasses (sample 1 and sample 2) respectively.

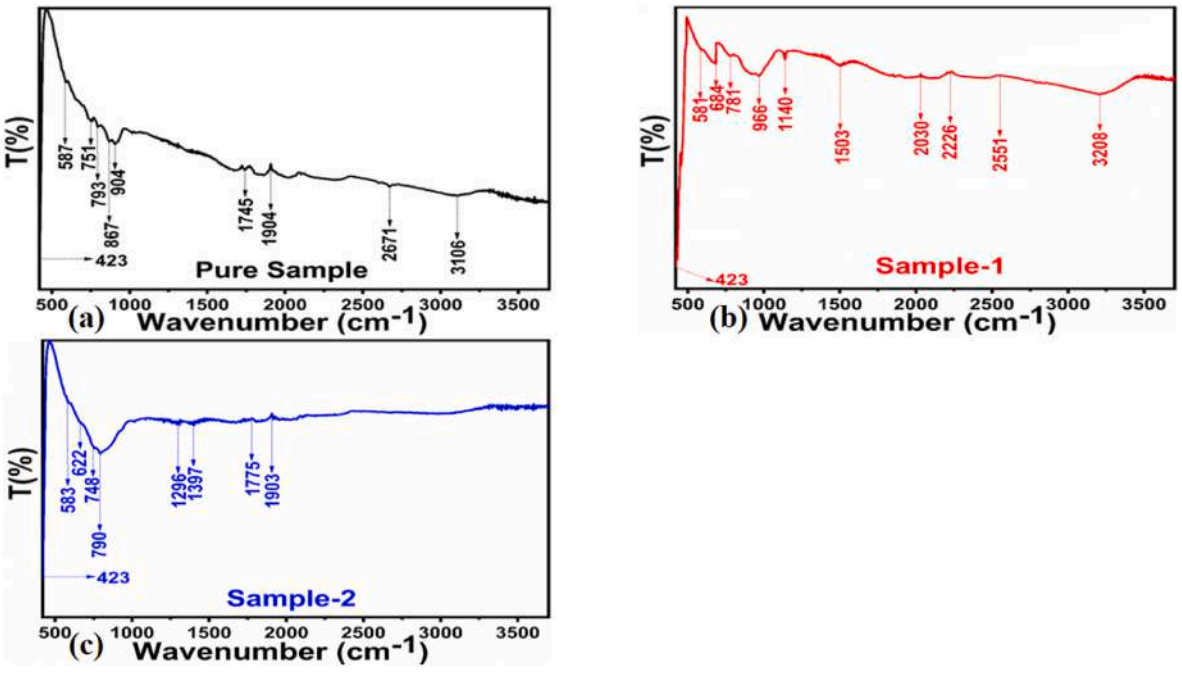

Fig. 5. FTIR spectra (a) pure Co_3O_4 without rotten grape (b,c) Co_3O_4 mediated with 1 mL and 2 mL of rotten grape (sample 1 and sample 2).

contributed to the significant variation in optical band gap energy in grape fruit extract, including reduced particle size, impurity energy levels, morphological changes, crystal defects, and synthetic route. The optical band gap values of the pure and grape fruit extract mediated Co_3O_4 nanostructures (samples 1 and 2) were 3.21 eV, 2.55 eV, and 2.89 eV, respectively.

3.2. Supercapacitor performance evaluation of grape fruit juice extract assisted Co_3O_4 nanostructures

For the preliminary supercapacitor investigations using cyclic voltammetry, three electrodes were used, with grape fruit extract derived Co_3O_4 nanostructures used as anode electrodes. We analyzed the capacitance behavior of grape fruit extract assisted Co_3O_4 nanostructures using CV analysis and compared them to pure Co_3O_4

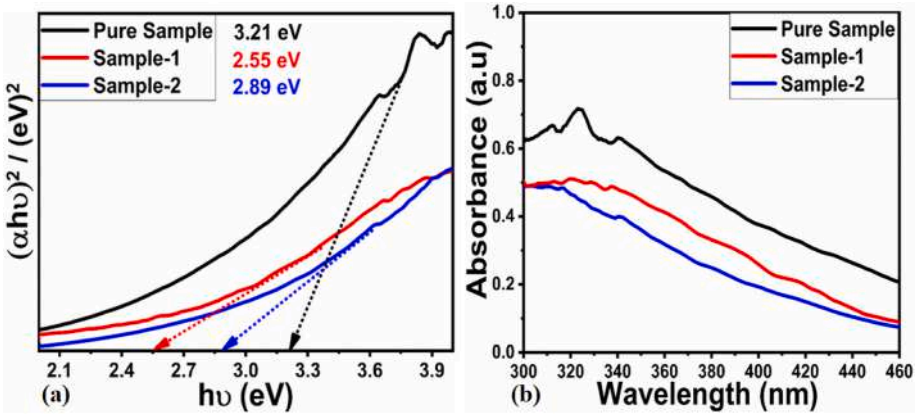

Fig. 6. (a) UV–visible absorption spectra of Co_3O_4 mediated with 1 mL and 2 mL of rotten grape (sample 1 and sample 2) and without rotten grape (pure Co_3O_4), (b) their corresponding Taucs plots of pure ,sample 1 and sample 2.

nanostructures as shown in Fig. 7a–d. As part of the recording process, CV curves were recorded against Hg/HgO at different scanning rates in a potential range between −0.1 V and 0.5 V using an electrolytic solution containing 3M KOH. CV study has revealed the surface kinetics controlled reaction between the electrode and electrolyte. By observing the wider and typical redox properties of CV curves, it is evident that pure and grapefruit-derived Co_3O_4 nanostructures exhibit significant pseudo capacitive properties. Co_3O_4 nanostructures derived from grape fruit extract exhibited enhanced reversibility of redox processes with increasing scan rate [55]. The CV curves have also demonstrated that the properties of grape fruit derived Co_3O_4 nanostructures are primarily influenced by pseudo capacitors rather than electrical double layer capacitors [56]. Nanostructured materials vary greatly in their morphology and size, which has a significant impact on the shape orientation of CV curves. Accordingly, the CV curves of the prepared Co_3O_4 nanostructures appear to be different from each other as shown in Fig. 7a–d. The galvanic charge-discharge curves of grapefruit derived Co_3O_4 nanostructures were also measured using the chronoamperometry method in an electrolyte containing 3M KOH at different current densities. As synthesized materials, Co_3O_4 nanostructures exhibited nonlinear GCD curves measured at different current densities such as 1.5, 2.5, 3.5, 4.5 and 5 A/g with ell defined pseudo capacitance properties [57]. Grape fruit extract has shown to significantly alter the morphology and size of Co_3O_4 nanostructures, thereby reducing the diffusion rate of hydroxide ions. Also, the use of grape fruit extract during the hydrothermal synthesis of Co_3O_4 nanostructures followed by calcination could add the carbon content which potentially enhanced the catalytic dispersion, resulting in reduced particle aggregation and good electrode stability. We estimated the specific capacitance, energy density, and power density using 2, 3, and 4 relations, respectively [57].

$$C_s = I/m \times \Delta T/\Delta V \quad (6)$$

$$E_d = C_s \times (\Delta V^2)/2 \quad (7)$$

$$P_d = E/\Delta T \quad (8)$$

Here, Cs represents specific capacitance, I current, m loading mass of electrode, ΔT discharge time, and ΔV as potential window.

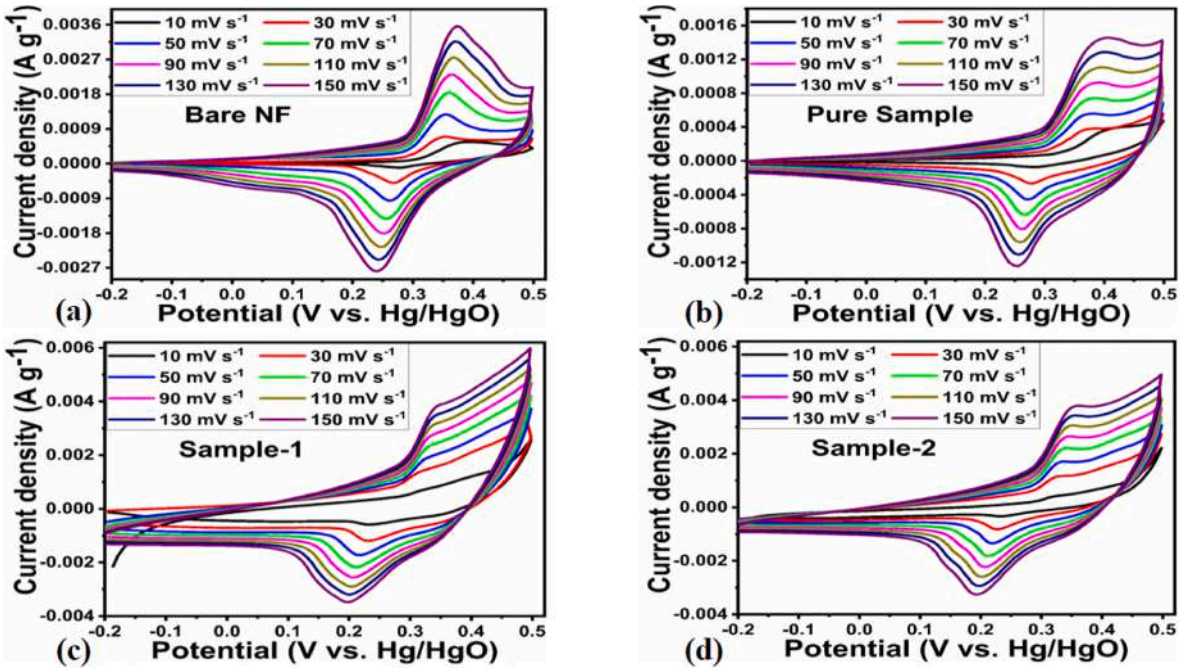

Fig. 7. CV polarization curves under t different sweeping scan rates in 3M KOH electrolyte using (a) bare nickel foam (NF), (b) pure Co_3O_4, (c, d) Co_3O_4 mediated with 1 mL and 2 mL of rotten Grape (sample 1 and sample 2) respectively.

Based on a comparative analysis of CV and GCD curves, it was concluded that the capacitance behavior of CV curves is higher due to well resolved Faradaic redox properties [58], whereas the lower capacitance of GCD curves is attributed to a lack of Faradaic redox processes at high current densities as shown in Fig. 8a–d. According to the GCD capacitance of various anode electrode materials, capacitance decreased with increasing current density [59]. As can be observed from the GCD curves, a significant voltage drop was observed due to the small equivalent series resistance and high current density resulting in polarization effects, which resulted in the inability to utilize the entire surface of the active electrode, resulting in reduced charge storage capacity. Furthermore, the calculated specific capacitance from GCD curves at various current densities, as shown in Fig. 9a, was calculated for bare nickel foam, pure Co_3O_4 nanostructures (sample 1), and grape fruit extract-derived Co_3O_4 nanostructures (sample 1, sample 2) as 50 F/g, 610 F/g, 867 F/g and 740 F/g, respectively, at 1.5 A/g. As shown in Fig. 8b, the energy density was estimated for the electrode materials studied. In the case of bare nickel foam, pure Co_3O_4, and grape fruit extract derived Co_3O_4 nanostructures (sample 1, sample 2), the values were 3, 11.3, 18.4 and 16.2 Wh/Kg, respectively. Using the specific capacitance and energy density values of sample 1, the GCD study indicates that this anode material has high potential for designing asymmetric supercapacitors, so it is necessary to examine the retention percentage and columbic efficiency of sample 1 as shown in Fig. 9c–d. Fig. 9c–d illustrates the electrochemical stability of sample 1 over 40000 GCD cycles at 1.5 A/g. The calculated values of specific retention percentage and columbic efficiency of sample 1 were 101.1 % and 99.9 % respectively during the repeatable GCD cycles at 1.5A/g. The cyclic stability of sample 1 indicates that it has a good cyclic stability and excellent pseudo capacitance properties. The excellent specific retention percentage of sample 1 could be assigned to the well dispersed nanoparticles and high compatibility with the surface of electrode, consequently outperform stability for maintaining the specific capacitance. Due to the improved redox reaction rate, sample 1 showed enhanced performance due to its unique shape, large surface exposure and utilization, and small diffusion of both hydroxide ions and electrons. It is clear from these observations that the grape fruit derived Co_3O_4 nanostructures possess excellent rate charge storage capability and are therefore capable of being used as an active electrode material for supercapacitors. Briefly, the performance of as developed supercapacitor is shown in Table 1. The comparative study of proposed supercapacitor was performed as given in Supplementary Table (S1). The analysis has suggested the proposed electrode material (sample 1) is simple, low cost, efficient ecofriendly compare to many of the developed electrode materials, hence it could be used as alternative material for the design of ream time energy storage device.

3.3. *Asymmetric supercapacitor performance of grape fruit assisted Co_3O_4 nanostructures*

In order to fabricate the asymmetric supercapacitor (ASC) device, two electrode cells were set up in 3M KOH aqueous solution in order to fabricate active electrode material from 1 mL of grape fruit derived Co_3O_4 nanostructures (sample 1). Before developing two electrodes, the three electrode supercapacitor performance of activated carbon (AC) was done as shown in Supplementary Figure (S1).The CV curves were measured at different for AC and the material has shown just limited capacitance behavior as shown, whereas the capacitance properties were noticed by the GCD cuvees at different current densities. Both CV and GCD behavior of AC were describing the poor electrochemical capacitance and energy density as the estimated values from GCD curves for the specific capacitance and energy density are shown in Supplementary Figure (S1). Based on these results, we integrated AC as cathode for the development of ASC. Co_3O_4 nanostructures were used as anode electrodes and activated carbon was used as cathode electrodes in sample 1. The ASC device was expressed in the form of Co_3O_4 GF//AC ASC. ASC CV curves at various scan rates and its corresponding GVD curves were also studied at various current densities as shown in Fig. 10. According to Fig. 10a, CV curves with scanning rates ranging from 10 mV/s to 150 mV/s showed a slight variation in the shape of the anode material, indicating potential electrochemical activity. ASC's GCD curves show a triangular shape without a plateau at various current densities of 1.5–5 A/g, confirming the useful and unique reversible redox reaction on the surface of the proposed anode material during ASC. According to Fig. 10b, the specific capacitance (Cs) of the ASC device was found to be 155 F/g at 1.5 A/g, which indicates excellent

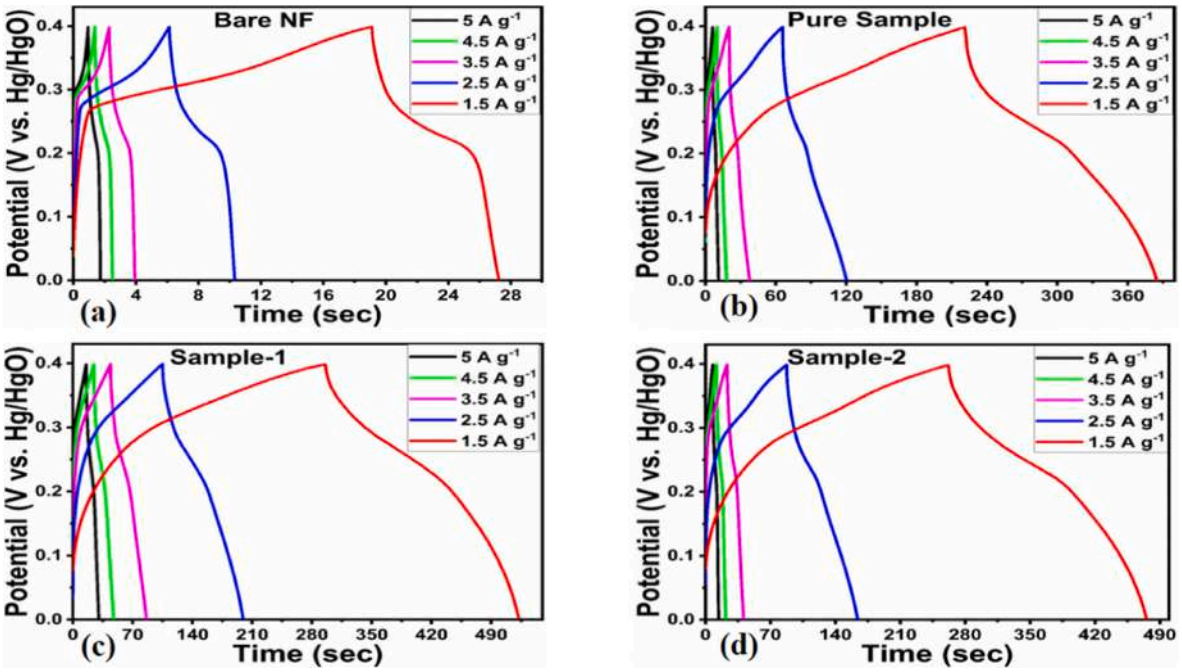

Fig. 8. Distinctive GCD curves obtained at various current densities in 3M KOH electrolyte using (a) bare nickel foam (NF), (b) pure Co_3O_4, (c, d) Co_3O_4 mediated with 1 mL and 2 mL of rotten Grape (sample 1 and sample 2) respectively.

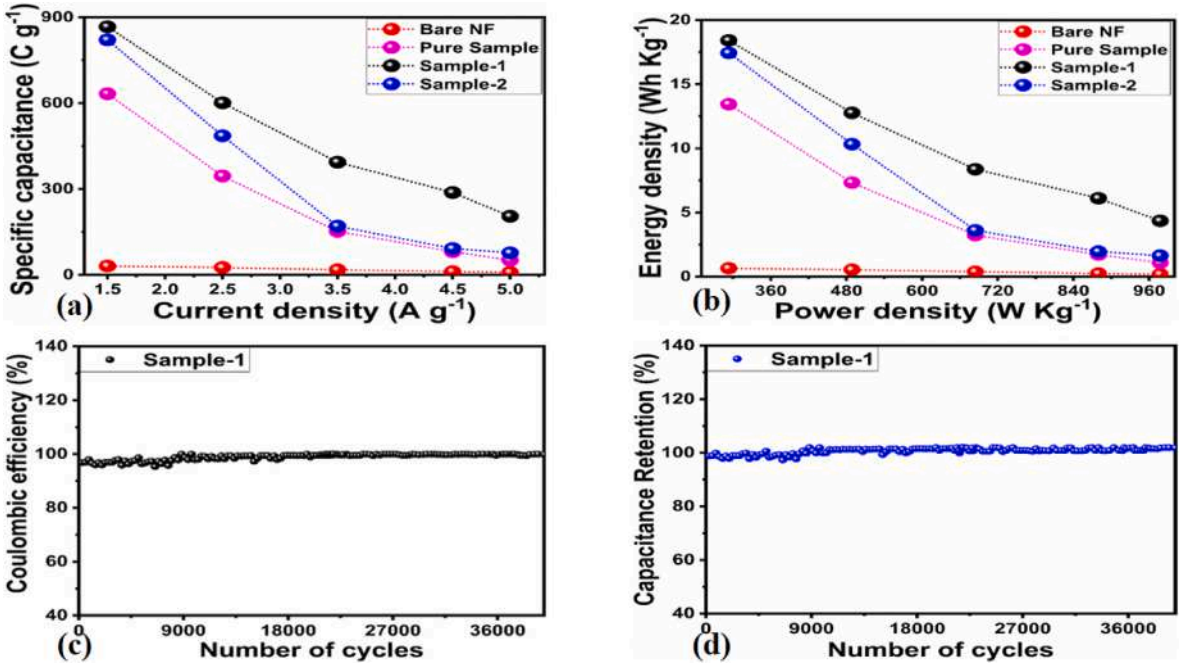

Fig. 9. (a) Estimated specific capacitance of bare nickel foam (NF), pure Co_3O_4, Co_3O_4 mediated with 1 mL and 2 mL of rotten grape (sample 1 and sample 2) respectively, (b) energy and power densities of calculated specific capacitance of bare nickel foam (NF), pure Co_3O_4, Co_3O_4 mediated with 1 mL and 2 mL of rotten grapes (sample 1 and sample 2) respectively, (c) columbic efficiency of sample 1 for 40000 GCD cycles at 1.5A/g, (d) percent capacitance retention of sample 1 during 40000 GCD cycles at 1.5 A/g current density.

Table 1
Calculated Supercapacitor parameters of sample 1 (Co_3O_4).

Sample	Current Density A g^{-1}	Specific Capacitance F g^{-1}	Energy Density (W h Kg^{-1})	Power Density (WKg^{-1})	Columbic Efficiency (%)	Capacitance Retention (%)
Sample 1 Co_3O_4	1.5	867	18.41	239.25	99.9 %	101.1 %
	2.5	601	12.76	488.75		
	3.5	393	8.36	684.25		
	4.5	287	6.11	879.75		
	5	204	4.34	977.50		

electrode performance of the anode material. In Fig. 9c, it can be seen that the energy density of the ASC device is approximately 3.2 Wh/Kg. At a current density of 1.5A/g about the anode material, repeatable 40000 GCD cycles were also conducted to estimate the columbic efficiency, and the results confirmed the columbic efficiency was 99 percent, whereas Fig. 10d and e illustrates the specific retention percentage of anode material as about 99 %. Due to the polarization effect, it was noticed that specific capacitance and energy density decreased with increasing current densities [59]. As demonstrated by the electrochemical performance of sample 1, the structure, morphology, surface chemical composition, and modified surface properties are crucial in driving the capacity of the anode electrode material to store charges. The excellent contribution of sample 1 towards the development of enhanced asymmetric devices could be indexed to the well-defined nanoparticles, modified surface properties, tunable optical band gap and uniform elemental composition of Co_3O_4 nanostructures. Through the use of rotten grape juice, it has provided the biomolecules that enhance the compatibility of structure with the electrode surface, resulting in an excellent specific capacitance retention percentage and cycling stability.

3.4. OER half-cell water splitting performance of grape fruit extract assisted Co_3O_4 nanostructure

A three-electrode cell set up in 1M KOH aqueous electrolytic solution was used to investigate the energy conversion aspects of different Co_3O_4 nanostructures derived from grape fruit extract. As shown in Fig. 11a, the OER polarization curves of pure and grape fruit derived Co_3O_4 nanostructures (sample 1, sample 2) were characterized by using LSV curves at a scan rate of 2 mV/s. According to LSV curves, the grape fruit modulates the OER activity of Co_3O_4 nanostructures compared to the pure system. According to Fig. 11a, sample 1 showed a lower OER onset potential than sample 2 and pure Co_3O_4 nanostructures, indicating that the surface properties and aspects of charge transfer were highly altered by the addition of 1 mL of grape fruit extract to the samples. In Fig. 11a, an overpotential of 290 mV at 10 $mAcm^{-2}$ was observed for sample 1, indicating that sample 2 and pure Co_3O_4 nanostructures experienced higher overpotentials at the same current density. The presence of well controlled phytochemical content during the synthesis of Co_3O_4 nanostructures by using 1 mL of grape fruit has drastically altered the electrochemical acridity during the OER half-cell water splitting process. These aspects of grape fruit indicate that it could be used to develop high performance electrocatalysts for efficient electrochemical water splitting in the future. Furthermore, the linear part of LSV curves was treated with Tafel equation fort the estimation of Tafel slopes in order to have possible deep insight on the OER mechanism. As shown in Fig. 11b, the results of the Tafel analysis have been presented. The Tafel slopes of the 1 mL and 2 mL derived Co_3O_4 nanostructures (sample 1, sample 2), as well as the pure system, were 80 $mVdec^{-1}$, 95 $mVdec^{-1}$, and 109 $mVdec^{-1}$, respectively. In sample 1, which had the lowest Tafel slope,

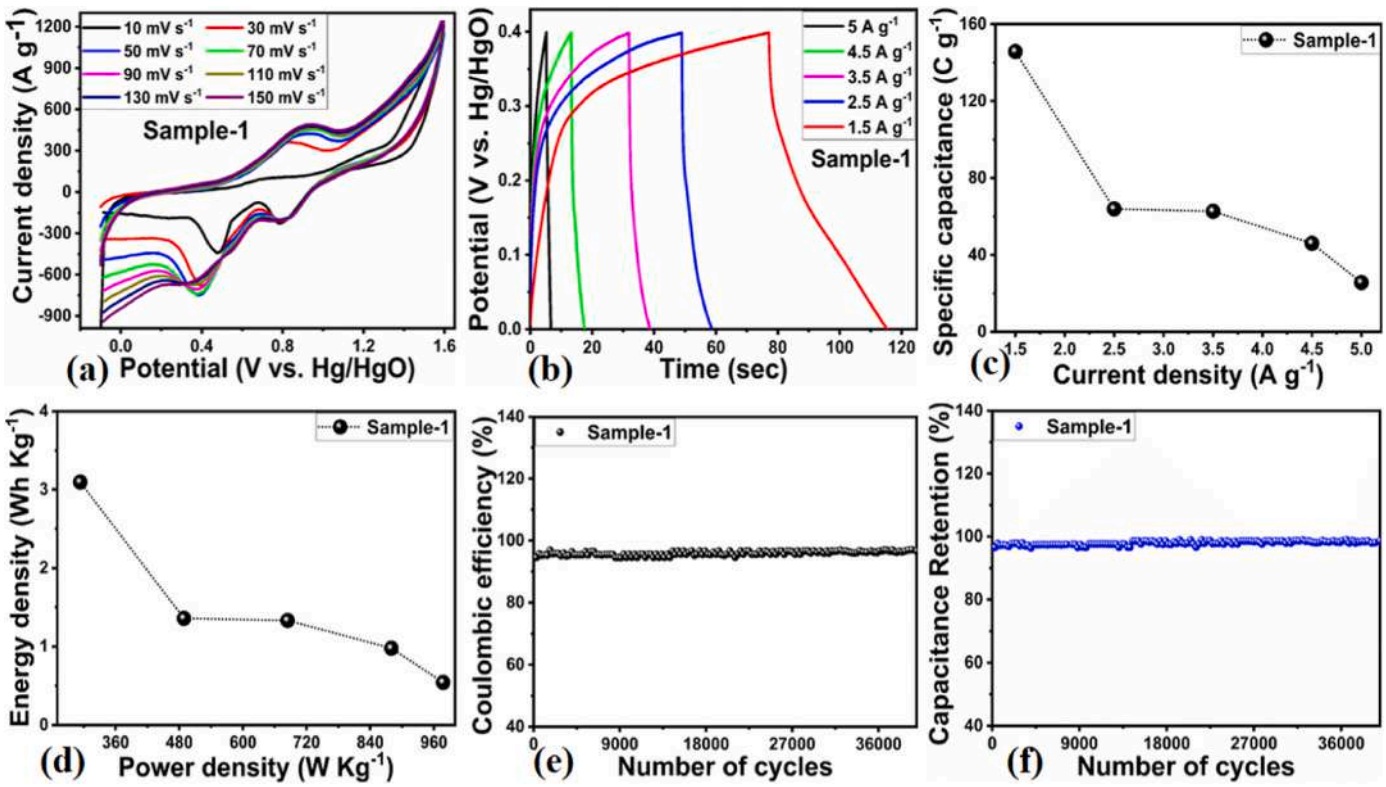

Fig. 10. (a) CV cycles of two electrode asymmetric supercapacitor based on anode material of Co_3O_4 mediated with 1 mL of rotten grape (sample 1) at various scan rates in 3M KOH aqueous solution and cathode of activated carbon (b) GCD cycles of anode electrode of Co_3O_4 prepared with 1 mL of rotten grape (sample 1) at various current densities in 3M KOH aqueous solution, (c) estimated specific capacitance of Co_3O_4 mediated with 1 mL of rotten grape fruit (sample 1), (d) energy and power densities of Co_3O_4 mediated with 1 mL of rotten grape (sample 1), (e) columbic efficiency of Co_3O_4 mediated with 1 mL of rotten grape (sample 1) using 40000 GCD repeatable cycles in 3M KOH aqueous solution, (f) Capacitance retention percentage of Co_3O_4 mediated with 1 mL of rotten grape (sample 1) for 40000 GCD repeatable cycle in 3M KOH aqueous solution.

the OER kinetics were highly favorable and again confirmed that grape fruit has significantly modulated the surface reaction properties of the sample. Tafel results for sample 1 could be attributed to the intrinsic electrochemical characteristics resulting from the reduced particle size, modified surface shape, and high surface-active sites exposed to the electrolyte. As shown in Fig. 11c, the stability of the sample was also assessed using the LSV curves before and after the chrono-potentiometer response time curve for the period of 40 h. The two LSV curves indicate that sample 1 has a high tendency to retain its onset potential and overpotential regardless of its durability performance over a long period of time. We also evaluated the durability of sample 1 during OER reaction using chronopotentiometry at a fixed current density of 20 $mAcm^{-2}$. Fig. 11d illustrates the measured response time curve for the period of 40 h. According to the durability test, sample 1 can be used for a long period of time without losing its overpotential. An excellent durability from a nonprecious catalyst verifies that the grape fruit played a significant role in enhancing the durability of sample 1 by eliminating agglomeration via the addition of carbon to the sample. Using non-Faradic CV curves at different scan rates, the electrochemical active surface area (ECSA) of sample 1 was calculated in order to demonstrate its superior OER activity compared to sample 2 and pure Co_3O_4 nanostructures. In Supplementary Figure (S2), we show the CV curves for bare nickel foam, pure Co_3O_4 nanostructures, and grape fruit derived Co3O4 nanostructures. The ECSA calculations suggested that the sample bare nickel foam, sample 1, sample 2 and pure Co_3O_4 nanostructures possessed values of 2.13 $nFcm^{-2}$, 1.5945 μFcm^{-2}, 1.5164 μFcm^{-2} and 1.33 $4\mu Fcm^{-2}$ respectively as shown in Supplementary Figure (S2) [60]. The sample 1 exhibited a significant amount of surface-active sites and it strongly supported the OER characterization in an aqueous electrolytic solution containing 1M KOH. Moreover, as shown in Fig. 11e, the interface charger transport of pure, sample 1, and sample 2 was also evaluated by EIS-based Nyquist plots. It has been stated in the existing literature that the semicircle arc at the low frequency area is related to the charge transfer resistance in given Nyquist plots [61–63]. Based on the fitted impedance data and the well-suited equivalent circuit, the estimated charge transfer resistance values for the pure, sample 1, and sample 2 were 94.37, 38.95, and 82.14 Ohms, respectively. As a result of the EIS results, sample 1 was found to have a low charge transfer resistance, indicating a fast charge transfer rate at the interface, which may have resulted in a rapid oxidation reaction under alkaline conditions [64]. ECSA and EIS results strongly support the excellent electrochemical performance of sample 1 of grape fruit derived Co3O4 nanostructures during the ASC and electrochemical water splitting tests. The OER study was compared with different published studies about the design of electrocatalysts as given in Supplementary Table (S2). The presented electrocatalyst based on sample is simple, cost effective, highly active and exhibiting low overpotential to many of the electrocatalysts. Hence, sample 1 based electrocatalyst could be used for the real time water splitting application. This improved electrochemical performance could be attributed to the effect of the phytochemicals present in 1 mM and 2 mL of grape extract which affect the shape structure, particle size, and surface modification of the particles, as well as the electrochemical properties of the particles.

4. Conclusions

Hydrothermal treatment of rotten grapefruit has modified the surface and shape structure of Co_3O_4 nanostructures. A structural analysis and an electrochemical analysis were conducted. In the XRD study, the cubic phase has been confirmed, variations in the two-theta indicate

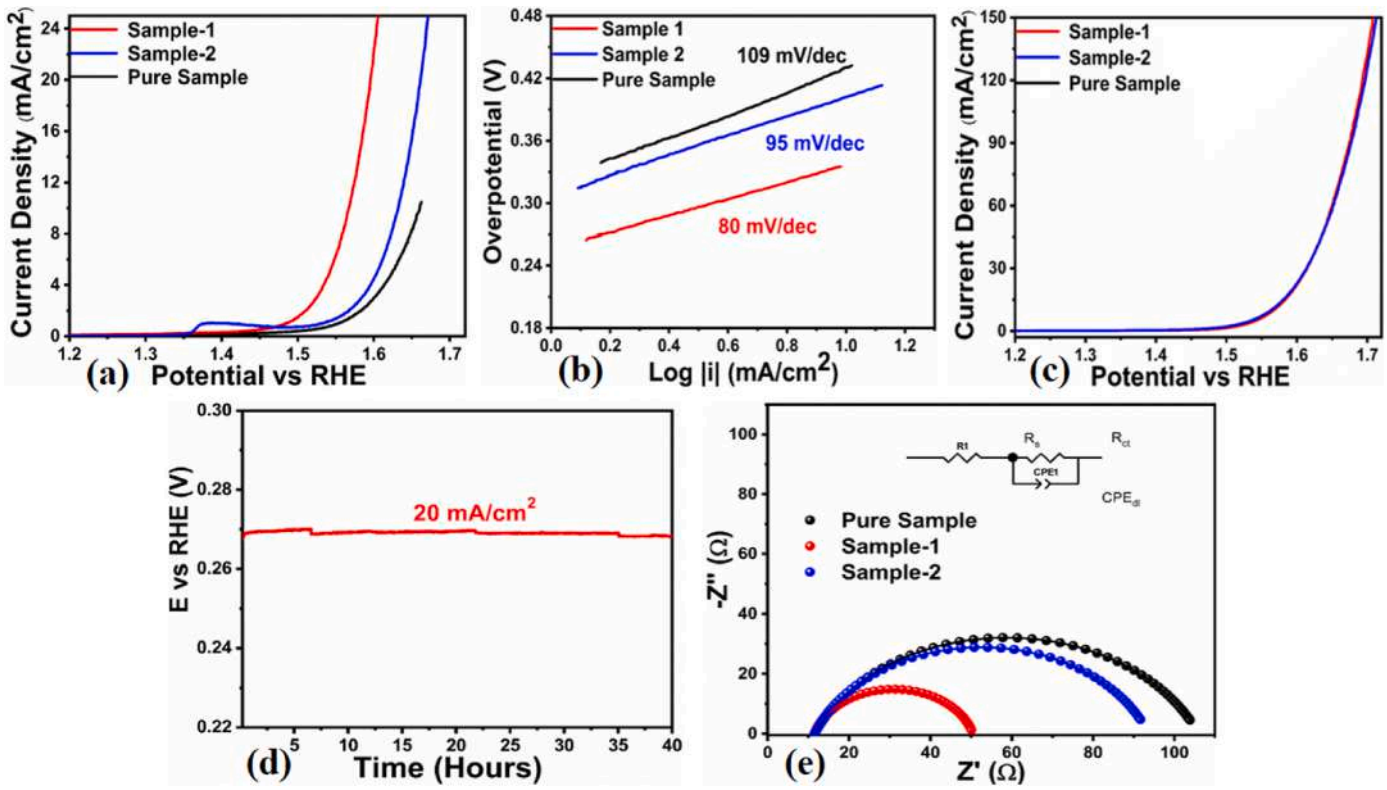

Fig. 11. (a) LSV polarization curves at 2 mV/s in 1M KOH aqueous solution of Co_3O_4 mediated with 1 mL and 2 mL of rotten grape (sample 1 and sample 2) and without rotten grape (pure Co_3O_4), (b) estimated Tafel slopes of from linear part of LSV curves through Tafel equation, (c) LSV curves before and after for illustration of durability test in 1M KOH of sample 1, (d) Chronopotentiometry curve of sample 1 for the durability of sample 1 in 1M KOH at constant current density of 20 mA/cm^2 (e) EIS derived Nyquist plots of Co_3O_4 mediated with 1 mL and 2 mL of rotten grape (sample 1 and sample 2) and without rotten grape (pure Co_3O_4) using frequency range 100 kHz to 0.1 Hz at an amplitude of 5 mV and OER onset potential vs (RHE) in 1.0M KOH aqueous solution.

defects, and the nanoparticles are trapped in the carbon species, as revealed by SEM. According to the UV–visible study, the optical band gap has been reduced. Among the different grape fruit extract volumes, 1 mL has demonstrated significant enhancement in the electrochemical properties of Co_3O_4 nanostructures in alkaline conditions. With 1 mL of grape fruit extract derived Co_3O_4 nanostructures, the OER study demonstrated an overpotential of 290 mV at 10 mAcm^{-2} and a Tafel slope of 80 mVdec^{-1}. Using 1.5 A/g current density in 3M KOH solution, the supercapacitor study reported a specific capacitance of 867 F/g. According to the results of the present research, the Co_3O_4 nanostructures prepared in the presence of rotten grape fruit extract during hydrothermal method are highly suitable for application as alternative electrode materials for OERs and supercapacitors.

CRediT authorship contribution statement

Asma Hayat: Validation, Resources, Formal analysis, Data curation. **Aneela Tahira:** Resources, Methodology, Investigation, Formal analysis. **Muhammad Ali Bhatti:** Methodology, Formal analysis, Data curation, Conceptualization. **Irum Naz:** Resources, Project administration, Investigation, Conceptualization. **Aqeel Ahmed Shah:** Resources, Methodology, Data curation. **Elmuez Dawi:** Writing – review & editing, Writing – original draft, Supervision, Funding acquisition, Formal analysis. **Matteo Tonezzer:** Writing – original draft, Visualization. **Ayman Nafady:** Project administration, Investigation, Formal analysis, Conceptualization. **Riyadh H. Alshammari:** Investigation, Formal analysis. **Zafar Hussain Ibupoto:** Writing – review & editing, Writing – original draft, Resources, Project administration.

Declaration of competing interest

The authors declare that they have no known competing financial interests or personal relationships that could have appeared to influence the work reported in this paper.

Data availability

Data will be made available on request.

Acknowledgment

The authors would like to gratefully acknowledge the Higher Education Commission Pakistan for partial support under the project NRPU/8350/8330. The authors extend their sincere appreciation to the Researchers Supporting Project number (RSP2024R442), King Saud University, Riyadh, Saudi Arabia, for partial funding of this work. Authors would also like to acknowledge partial funding of the Ajman University, Grant ID: DRG ref. 2023-IRG-HBS-2 (RESHUSC-001), RTG-2023-HBS-1.

Appendix A. Supplementary data

Supplementary data to this article can be found online at https://doi.org/10.1016/j.rineng.2024.102922.

References

[1] A.M. Omer, Energy Environment and Sustainable Development Renew and Sustainable Ener Revi, 12, 2008, pp. 2265–2300.
[2] B. Mahesh, A comprehensive review on current trends in greener and sustainable synthesis of ferrite nanoparticles and their promising applications, Results in Engineering 24 (2023) 101702.

[3] M. Mahmud, K.S. Rahman, M. Rokonuzzaman, et al., Lithium-ion battery thermal management for electric vehicles using phase change material: a review, Results in Engineering 16 (2024) 101424.
[4] M. Rostami, P. Rezvaninia, A. Amiri, et al., Hybrid nano-architectural engineering of Ti3C2Tx MXene heterostructures for supercapacitor applications: a reviews, Results in Engineering 7 (2024) 102227.
[5] J. Shen, J. Gao, L. Ji, et al., Three-dimensional interlinked Co_3O_4-CNTs hybrids as novel oxygen electrocatalyst, Appl. Surf. Sci. 497 (2019) 143818.
[6] L. Zhang, J. Xiao, H. Wang, et al., Carbon-based electrocatalysts for hydrogen and oxygen evolution reactions, ACS Catal. 7 (2017) 7855–7865.
[7] Y. Cheng, Advances in electrocatalysts for oxygen evolution reaction of water electrolysis-from metal oxides to carbon nanotubes, Progress in natural science Mater internati 25 (2015) 545–553.
[8] G. Wu, A. Santandreu, W. Kellogg, et al., Carbon nanocomposite catalysts for oxygen reduction and evolution reactions from nitrogen doping to transition-metal addition, Nano Ener 29 (2016) 83–110.
[9] C. Wolfram, O. Shelef, P. Gertler, How Will Energy Demand Develop in the Developing World Jour of Econo Perspectives, 26, 2012, pp. 119–138.
[10] E. Shove, G. Walker, What is energy for Social practice and energy demand, Theory, cultu & socie 31 (2014) 41–58.
[11] P.J. Hall, M. Mirzaeian, S.I. Fletcher, et al., Energy storage in electrochemical capacitors designing functional materials to improve performance, Ener & Enviro Scie 3 (2010) 1238–1251.
[12] Y. Lu, Z. Zhang, X. Liu, et al., $NiCo_2S_4$/carbon nanotube nanocomposites with a chain-like architecture for enhanced supercapacitor performance, CrystEngComm 18 (2016) 7696–7706.
[13] L. Tripathi, A. Mishra, A.K. Dubey, et al., Renewable energy: an overview on its contribution in current energy scenario of India, Ren. and Sus. En. Revi. 60 (2016) 226–233. Tripathi C, Baredar P.
[14] L.L. Zhang, X. Zhao, Carbon-based materials as supercapacitor electrodes, Chemi soc revi 38 (2009) 2520–2531.
[15] X. Chen, R. Paul, L. Dai, Carbon-based supercapacitors for efficient energy storage, Natio Scien Revi 4 (2017) 453–489.
[16] S. Banerjee, K.K. Kar, Conducting polymers as electrode materials for supercapacitors. Handbook of Nanocomposite Supercapacitor Materi II Performa, 2020, pp. 333–352.
[17] Y. Han, L. Dai, Conducting polymers for flexible supercapacitors, Macromol. Chem. Phys. 220 (2019) 1800355.
[18] Y. Wang, J. Guo, T. Wang, et al., Mesoporous transition metal oxides for supercapacitors, Nanomateri 5 (2015) 1667–1689.
[19] L. Miao, Z. Song, D. Zhu, et al., Recent advances in carbon-based supercapacitors, Materia Advanc 1 (2020) 945–966.
[20] A. Borenstein, O. Hanna, R. Attias, et al., Carbon-based Composite Materials for Supercapacitor Electrodes: a Review Jour of Materi Chemi, 5, 2017, pp. 12653–12672.
[21] M. Abdah, M.A. Aizat, N.H. Azman, et al., Review of the use of transition-metal-oxide and conducting polymer-based fibres for high-performance supercapacitors, Materi & Design 186 (2020) 108199.
[22] M.J. Dunlop, R. Bissessur, Nanocomposites based on graphene analogous materials and conducting polymers a revi Journ of materi Scien 55 (16) (2020) 6721–6753.
[23] M. Guan, Q. Wang, X. Zhang, et al., Two-dimensional transition metal oxide and hydroxide-based hierarchical architectures for advanced supercapacitor materials, Fronti in Chem 8 (2020) 390.
[24] R. Gao, D. Yan, Recent development of Ni/Fe-based micro/nanostructures toward photo/electrochemical water oxidation, Adva Ener Mater 10 (11) (2020) 1900954.
[25] Z. Wu, Y. Zhu, X. Ji, $NiCo_2O_4$-based materials for electrochemical supercapacitors, Jour of Mater Chemi 2 (36) (2014) 14759–14772.
[26] A.K. Mittal, Y. Chisti, U.C. Banerjee, Synthesis of metallic nanoparticles using plant extracts, Biotechno advan 31 (2) (2013) 346–356.
[27] N.D. Kandpal, N. Sah, R. L oshali, et al., Co-precipitation method of synthesis and characterization of iron oxide nanoparticles, J Sci Ind Res 73 (2014) 87–90.
[28] N. Bayal, P. Jeevanandam, Synthesis of TiO_2– MgO mixed metal oxide nanoparticles via a sol–gel method and studies on their optical properties, Cerami Internat 40 (10) (2014) 15463–15477.
[29] A. Salimi, H. Mamkhezri, R. Hallaj, Electrochemical detection of trace amount of arsenic (III) at glassy carbon electrode modified with cobalt oxide nanoparticles, Sens. and Actua Chemi 129 (1) (2008) 246–254. Soltanian S.
[30] M.M. Titirici, M. Antonietti, A. Thomas, A generalized synthesis of metal oxide hollow spheres using a hydrothermal approach, Chemis of materi 18 (16) (2006) 3808–3812.
[31] J. Singh, T. Dutta, K.H. Kim, et al., Green synthesis of metals and their oxide nanoparticles applications for environmental remediation, Jour of nano biotechnology 16 (2018) 1–24.
[32] N. Basavegowda, A. Idhayadhulla, Y.R. Lee, Preparation of Au and Ag nanoparticles using Artemisia annua and their in vitro antibacterial and tyrosinase inhibitory activities, Materi Scie Engineer 1 (43) (2014) 58–64.
[33] Z.U. Khan, A. Khan, Y. Chen, et al., Biomedical applications of green synthesized Nobel metal nanoparticles, Journal of Photochemistry and Photobiol Biolog 1 (173) (2017) 150–164.
[34] V.P. Haritha, V. Haridas, K.V. Snisha, et al., β-Co (OH) 2–Co3O4/Graphene Oxide 3D-Nanoarchitecture modified electrode for electrochemical sensing and energy storage applications, Results in Engineering 19 (2023) 101391. Binitha NN.
[35] A. Akter, S.A. Razzaque, M.A. Haque, et al., Construction of F-doped Co3O4/Co3O3. 69F0. 31 nanocomposite for boosting photocatalytic removal of organics from industrial waste H2O under visible-light, Results in Engineering 16 (2022) 100672.
[36] G. Song, L. Mu, P. Qiao, et al., Oxygen vacancies modulated Co3O4 toward highly efficient electrooxidation of 5-hydroxymethylfurfural, Results in Engineering 20 (2023) 101606.
[37] S. Dubey, J. Kumar, A. Kumar, et al., Facile and green synthesis of highly dispersed cobalt oxide (Co_3O_4) nano powder Characterization and screening of its eco-toxicity, Advan Powr Techno 29 (11) (2018) 2583–2590.
[38] S. Palani, U.S. Veerasamy, Y. Mona, et al., Facile synthesis of rGO nanosheet encapsulated Ni2V2O7 nanorods for energy storage applications, Results in Engineering 22 (2024) 102134.
[39] A. Purwanto, M. Diantoro, A. Subagio, et al., Using tea waste to produce a high-performance lithium-ion capacitor—bio-graphite/Li4Ti5O12 (LTO), Results in Engineering 22 (2024) 102156.
[40] N. Girija, S.S. Kuttan, B.N. Nair, et al., Morphology control in nickel cobaltite synthesised via solution routes for electrochemical applications, Results in Engineering 15 (2022) 100536.
[41] I. Bibi, N. Nazar, M. Iqbal, et al., Green and eco-friendly synthesis of cobalt-oxide nanoparticle: characterization and photo-catalytic activity, Advan Pow Technol 28 (9) (2017) 2035–2043.
[42] A. Diallo, A.C. Beye, T.B. Doyle, et al., Green synthesis of Co3O4 nanoparticles via Aspalathus linearis physical properties, Green Chemistry Lett and Reviews 8 (3–4) (2015) 30–36.
[43] P.D. Sarvalkar, A.S. Jamadar, A.B. Magdum, et al., Biogenic synthesis of Co3O4 nanoparticles from Aloe barbadensis extract: antioxidant and antimicrobial activities, and photocatalytic degradation of azo dyes, Results in Engineering 22 (2024) 102094.
[44] T. Maier, A. Schieber, D.R. Kammerer, et al., Residues of grape (Vitis vinifera L.) seed oil production as a valuable source of phenolic antioxidants, Fo Chemis 112 (3) (2009) 551–559.
[45] K. Amarnath, N.L. Mathew, J. Nellore, et al., Facile synthesis of biocompatible gold nanoparticles from Vites vinefera and its cellular internalization against HBL-100 cells, Canc nanotechn 2 (2011) 121–132. Siddarth CRV, Kumar J.
[46] S. Ramanathan, S. Moorthy, S. Ramasundaram, et al., Grape seed extract assisted synthesis of dual-functional anatase TiO2 decorated reduced graphene oxide composite for supercapacitor electrode material and visible light photocatalytic degradation of bromophenol blue dye, ACS Omega 6 (23) (2021) 14734–14747.
[47] Y.Y. Liang, S.J. Bao, H.L. Li, Nanocrystalline nickel cobalt hydroxides/ultrastable Y zeolite composite for electrochemical capacitors, Jour of Sol Stat Electrochem 11 (2007) 571–576.
[48] Y. Li, K. Huang, S. Liu, et al., Meso-macroporous Co_3O_4 electrode prepared by polystyrene spheres and carbowax templates for supercapacitors, Jour of Sol Sta Electrochemi 15 (2011) 587–592.
[49] M. Aghazadeh, Electrochemical preparation and properties of nanostructured Co_3O_4 as supercapacitor material, Jour of App Electro chemi 42 (2012) 89–94.
[50] N.N. Binitha, P.V. Suraja, Z. Yaakob, Simple synthesis of Co_3O_4 nanoflakes using a low temperature sol–gel method suitable for photodegradation of dyes, Jour of sol-gel scie and technol 53 (2011) 466–469.
[51] S. Farhadi, K. Pourzare, S. Sadeghinejad, Simple preparation of ferromagnetic Co_3O_4 nanoparticles by thermal dissociation of the [Co II $(NH_3)6$] $(NO_3)_2$ complex at low temperature, Jour of Nano struc in Chemis 3 (2013) 1–7.
[52] H. Chen, W. Li, M. He, et al., Vertically oriented carbon nanotube as a stable frame to support the Co0.85Se nanoparticles for high performance supercapacitor electrode, Jour of Alloys and Compounds 855 (2021) 157506.
[53] M. Manickam, V. Ponnuswamy, C. Sankar, et al., Structural, optical, electrical and electrochemical properties of Fe: Co_3O_4 thin films for supercapacitor applications, Jour of Materia Scien Materi in Electroni (2017) 18951–18965.
[54] R.S. Reena, A. Aslinjensipriya, M. Jose, et al., Investigation on structural, optical and electrical nature of pure and Cr-incorporated cobalt oxide nanoparticles prepared via co-precipitation method for photocatalytic activity of methylene blue dye, Jour of Mater Science Materials in Electronics 31 (24) (2020) 22057–22074.
[55] H.J. Choi, S.M. Jung, J.M. Seo, et al., Graphene for energy conversion and storage in fuel cells and supercapacitors, Nano Energy 1 (4) (2012) 534–551.
[56] S.K. Meher, G.R. Rao, Ultralayered Co_3O_4 for high-performance supercapacitor applications, The Jour Physi Chemis 115 (31) (2011) 15646–15654.
[57] X. Li, G. Wang, X. Wang, et al., Flexible supercapacitor based on MnO_2 nanoparticles via electrospinning, Jour Materi Chemis 1 (35) (2013) 10103–10106.
[58] M. Kumar, A. Subramania, K. Balakrishnan, Preparation of Electrospun Co3O4 Nanofibers as Electrode Material for High Performance Asymmetric Supercapaci Electro Chim Acta149, 2014, pp. 152–158.
[59] J. Xu, L. Gao, J. Cao, et al., Preparation and electrochemical capacitance of cobalt oxide (Co_3O_4) nanotubes as supercapacitor material, Electrochim. Acta 56 (2) (2010) 732–736.
[60] Y.T. Lu, Y.J. Chien, C.F. Liu, et al., Active site-engineered bifunctional electrocatalysts of ternary spinel oxides, M 0.1 Ni 0.9 Co_2O_4 (M: Mn, Fe, Cu, Zn) for the air electrode of rechargeable zinc–air batteries, Jour of Mater Chemis A (39) (2017) 21016–21026.
[61] H.J. Lee, D.H. Park, W.J. Lee, et al., Mesoporous spinel Ir-doped NiCo2O4 nanostructure as an efficient catalyst for oxygen evolution reaction, Appl Catalys A General 626 (2021) 118377.
[62] S.K. Li, A.Y. Chen, Y.Q. Chai, et al., Electrochemiluminescence aptasensor based on cascading amplification of nicking endonuclease-assisted target recycling and

rolling circle amplifications for mucin 1 detection, Electrochim. Acta 212 (2016) 767–774.
[63] A.J. Laghari, U. Aftab, A. Tahira, et al., MgO as promoter for electrocatalytic activities of Co_3O_4–MgO composite via abundant oxygen vacancies and Co^{2+} ions towards oxygen evolution reaction, International Jour of Hydr Ener 48 (34) (2023) 12672–12682.
[64] X. Long, J. Li, S. Xiao, et al., A strongly coupled graphene and FeNi double hydroxide hybrid as an excellent electrocatalyst for the oxygen evolution reaction, Angewandte Chemie Internati Edition 53 (29) (2014) 7584–7588.